Revista de Informática Teórica e Aplicada - RITA - ISSN 2175-2745
Vol. 32, Num. 1 (2025) 114-120

RESEARCH ARTICLE

Bulldogs Nose Detection using Deep Learning

Detecção das Narinas de Buldogues utilizando Aprendizado Profundo

Joyce Katiuccia Medeiros Ramos Carvalho[1], Pedro Henrique Neves da Silva[2], Sandra Adriana Uhry[1], Gustavo da Silva Andrade[2], Gisele Braziliano de Andrade[1], Hemerson Pistori[1], Newton Loebens[3]*

Abstract: An animal nose identification system could allow efficient monitoring of pets, and it can be used in applications such as identifying animal breeds or possible diseases and/or injuries. For that, a bulldog image dataset was build from French bulldogs. To carry out the validation through cross-validation, 10 folds (K-folds) were created. Afterward, five convolutional neural networks (CNN) were trained with our dataset to identify the nose: Faster R-CNN (Region-based CNN), SABL (Side-Aware Boundary Localization), RetinaNet (ResNet50+FPN), VFNet (VarifocalNet), and ATSS (Adaptive Training Sample Selection). Faster R-CNN, SABL, RetinaNet, VFNet and ATSS were used for training in the first phase, while ATSS, Faster R-CNN, ATSS and SABL in the second. The results showed that the ATSS network obtained the highest values of mAP and Accuracy in the first phase. Moreover, SABL network achieved the highest values of mAP50, mAP75, Recall, F-Score and Accuracy at the end of the second phase.
Keywords: Computer Vision — Neural Networks — Brachycephalic Obstructive Airway Syndrome — Stenotic Nares — Bulldogs Nose

Resumo: Um sistema de identificação de nariz de animal pode permitir o monitoramento eficiente de animais de estimação, e pode ser usado em aplicações como identificação de raças de animais ou possíveis doenças e/ou ferimentos. Para isso, um conjunto de dados de imagens de bulldog foi construído a partir de bulldogs franceses. Para realizar a validação por meio de validação cruzada, 10 dobras (K-folds) foram criadas. Depois, cinco redes neurais convolucionais (CNN) foram treinadas com nosso conjunto de dados para identificar o nariz: Faster R-CNN (CNN baseada em região), SABL (Side-Aware Boundary Localization), RetinaNet (ResNet50+FPN), VFNet (VarifocalNet) e ATSS (Adaptive Training Sample Selection). Faster R-CNN, SABL, RetinaNet, VFNet e ATSS foram usados para treinamento na primeira fase, enquanto ATSS, Faster R-CNN, ATSS e SABL na segunda. Os resultados mostraram que a rede ATSS obteve os maiores valores de mAP e Accuracy na primeira fase. Além disso, a rede SABL atingiu os maiores valores de mAP50, mAP75, Recall, F-Score e Precisão no final da segunda fase.
Palavras-Chave: Visão Computacional — Redes Neurais — Síndrome Obstrutiva das Vias Aéreas dos Braquicefálicos — Narinas Estenóticas — Nariz de Buldogue

[1] *Universidade Católica Dom Bosco (UCDB), Brazil*
[2] *Universidade Federal de Mato Grosso do Sul (UFMS), Brazil*
[3] *Universidade Federal do Pampa (UNIPAMPA), Brazil*
***Corresponding author**: newtonloebens@unipampa.edu.br
DOI: http://dx.doi.org/10.22456/2175-2745.143541 • **Received:** 24/10/2024 • **Accepted:** 02/12/2024

1. Introduction

Since the domestication of wolves, mankind have influenced the emergence of new canine breeds and genetic variability, through the artificial selection of aptitudes, in order to obtain animals bred according to their objectives. This occurs by altering the physical or aesthetic appearance, influencing attributes such as bone conformation, coat, weight and musculature, which eventually can cause problems for the health of these animals. The emergence of brachycephalic canine breeds can be related to the search for animals for combat, due to the belief that the shape of their head would provide a stronger bite [10].

The Brachycephalic Obstructive Airway Syndrome (BOAS) is due to congenital anatomical malformations [11] that cause several problems due to shortening and enlargement of the skull [12] and muzzle, and consequently of the underlying bones [10]. The conformational changes led to the occurrence of nostril stenosis, elongation and increase in the thickness of the soft palate, tracheal hypoplasia, enlarged tonsils, eversion of laryngeal saccules, collapse of the larynx and/or trachea and increase in nasopharyngeal turbinates, which may result in obstruction. of the airways [12][18][19].

These alterations may present in isolation or in combination, and in different degrees of morbidity [14, 15, 1, 22]. As a result of the anatomical changes that obstruct the airways, clinical signs such as snoring, respiratory distress, exercise intolerance, rales, tachypnea, hyperthermia, dyspnea and cyanosis appear [13, 12, 20, 23].

About 60% of veterinarians and owners do not know how to recognize the clinical signs of this disease, impairing early treatment. However, in recent years, there has been growing concern about the welfare of animals with this syndrome [17, 16, 20, 24, 22]. Physical examination, the patient's medical history, and an evaluation under general anesthesia are used for the diagnosis of BOAS. However, these methods are subjective or invasive, making early diagnosis and treatment difficult [21]. Thus, the development of new methods for non-invasive and objective measurements of respiratory function in brachycephalic dogs is necessary.

This paper contemplates some steps taken to detect the nose of bulldogs, from taking images to create our dataset to train the networks. The contribution of this work is a novel annotated dataset and the empirical evaluation of deep learning techniques to attack a problem that has not been attacked before in this kind of image.

2. Related Works

The bovine snout has unique characteristics that can be compared to fingerprints in humans, making it possible to track the cattle through non-invasive ways by identifying the snout patterns. In the research of [31], the main goal was to collect and publish a quality dataset for snout images of beef cattle and to evaluate and compare the recognition performance of individual beef cattle with a variety of deep learning models. 4923 snout images of 268 feedlot cattle (> 12 images per animal, on average) were obtained with a digital camera and processed to form the input dataset for 59 deep learning image classification models to identify individual cattle. In the benchmarking, the best performance in terms of accuracy was obtained by VGG16_BN (98.7%) and the fastest processing speed was obtained by MobileNetV3_Small (28.3 ms/image), both with data augmentation and weighted cross-entropy as loss function, demonstrating the great potential of deep learning applications for individual identification of cattle and is favorable for precision beef cattle management.

Aiming to identify the face of the herd of dairy cows using deep learning and computer vision techniques, [29] proposed, through video analysis, recognition carried out in four steps: face detection, face cropping, face encoding and face lookup. For this purpose, three deep learning models were used Face detector, Landmark predictor and Face encoder. These models were adjusted through transfer learning on a dataset of dairy cows from a farm on the Dookie campus at the University of Melbourne, Australia. The result of this study demonstrated 84% overall accuracy of videos from 89 different dairy cows.

Computer vision, through the method of facial recognition and patterns observed through digital images and videos, has been used in the study of the conservation of endangered animals, such as the giant panda. Making a breakthrough in assessing the effectiveness of conservation and management strategies a fully automatic deep learning algorithm consisting of a sequence of deep neural networks (DNNs) used for panda face identity detection, segmentation, alignment and prediction was developed in [30]. To develop and evaluate the algorithm, the largest panda image dataset containing 6,441 images of 218 different pandas was established. The algorithm achieved 96.27% accuracy in panda recognition and 100% accuracy in detection.

The authors of [28] used a trained and tested CNN with thoracolumbar magnetic resonance (MR) images of 500 dogs, weighted in T1 and T2 in the sagittal and transverse planes. This network was trained with 2693 RM images from 375 dogs and tested with 7695 MR images of 125 dogs. The dataset consisted of 39 dogs with unremarkable MR images and 461 dogs demonstrating spinal cord pathologies such as: 284 dogs with intervertebral disc extrusion (IVDE), 38 dogs with intervertebral disc protrusion (IVDP), 108 dogs with fibrocartilaginous embolism (FCE) and acute non-compressive extrusion of the nucleus pulposus (ANNPE), 13 dogs with syringomyelia and 18 dogs with neoplasia.

The network performed best in detecting IVDPs on sagittal T1-weighted images with a sensitivity of 100% and specificity of 95.1%. In the detection of IVDEs, in the sagittal T2-weighted images, there was also a good performance with sensitivity of 90.8% and specificity of 98.98%. In this study, the network response to FCEs and ANNPEs detected a sensitivity of 62.22% and a specificity of 97.90% on sagittal T2-weighted images and with a sensitivity of 91% and specificity of 90% on cross-sectional T2-weighted images, respectively. For the detection of neoplasms and syringomyelia, the network did not perform well because it presented insufficient data for training or even had difficulties with hyperintensities in T2 images. This study showed the possibility of training a CNN network for recognition and differentiation of various spinal cord pathologies in canine magnetic resonance imaging.

3. Materials and Methods

To carry out the bulldog nose detection experiment, some initial steps were necessary before starting the pre-processing of the images and their use for training and testing. The workflow, on Figure 1, was executed as follows: (A) A new bulldog dataset was build and (B) Images were annotated in the nose region, Subsection 3.1; (C) Neural network training performed based on the annotated images, Subsection 3.2; (D)

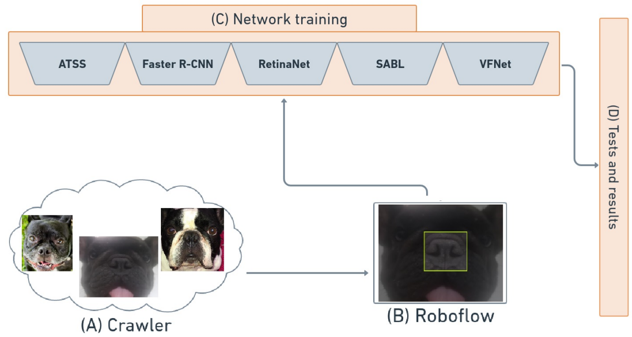

Figure 1. Experimental workflow followed in the first phase of the research. The images were downloaded from the internet (A), annotated in the nose region (B) and used for training and testing the Faster R-CNN, RetinaNet, VFNet, ATSS and SABL networks (C), where the results were generated (D).

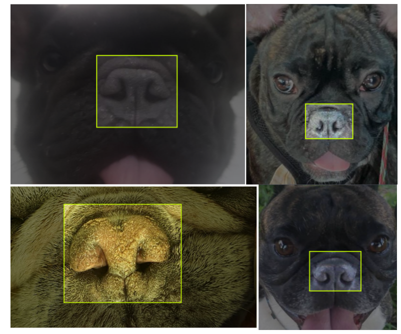

Figure 2. Images annotated from dataset.

The images were tested, generating results, Subsection 3.3.

3.1 Our dataset

The dataset used in this research was built with 110 free domain images of French and English bulldogs, obtained from the internet, and 54 photographic images of the frontal projection obtained only from French bulldogs, of both genders, age between 2 and 10 years old, mean of approximately 5 years old and standard deviation of 3 years, in the city of Campo Grande, MS. The downloaded RGB images, with resolution ranging from 255×225 pixels to 2048×1485 pixels, were chosen in such a way that not only images that facilitate the learning of the algorithms were selected, but also images where the dogs appeared a little in profile or even with the tongue over the mouth and part of the nose. This choice aimed at better training through networks in the execution of processes based on different types of data. To perform our images, the face of each animal was photographed with the aid of an iPhone XS smartphone or with a Samsung Note 10, at a distance of approximately 40 centimeters and with resolution of 4608×2592. When capturing the images, those responsible for the animals signed a free and informed consent form, agreeing with the inclusion of photographic images of the animal's faces in the research, in addition to filling out a questionnaire about the respiratory condition of each animal.

3.2 Deep Learning

With the images properly annotated, as shown in Figure 2, the training and testing stage were divided into 2 phases. In the first phase, the 110 images downloaded from the internet were separated into 5 different folds [6], according to the K-fold cross-validation sampling technique [5]. The result of this first phase determined which networks would be used in the second phase, in which the 110 images would be used for training, without cross-validation, and the 54 performed images for testing.

In this study, the ensemble of models was trained on a dataset of bulldog images using various convolutional neural networks (CNNs) to detect the dogs' noses. The networks were trained for a number of epochs ranging from 10 to 30. However, the metrics stabilized after 15 epochs, making further training unnecessary. The Intersection over Union (IoU) threshold was set to 0.3, which means that predicted bounding boxes with at least 30% overlap with the ground truth were considered correct. A learning rate of 0.01 was used and the primary metric used to evaluate the performance was mean Average Precision (mAP), a standard measure for object detection tasks. The training was conducted in Google Colab PRO, using a T4 GPU and 32GB of RAM. For the training of these images, we used five convolutional neural networks (CNN): Faster R-CNN (Region-based Convolutional Neural Networks) [2], SABL (Side-Aware Boundary Localization) [4], RetinaNet (ResNet50 + FPN) [7], VFNet (VarifocalNet) [8], and ATSS (Adaptive Training Sample Selection) [9].

The Faster R-CNN neural network has two execution modules, the first, called Region Proposal Network (RPN), is responsible for obtaining characteristics and producing a set of proposals with its candidate objects, and the second, utilizes the Fast R-CNN detector to identify, or classify, the target objects providing their assertion probability [3]. Just as Faster R-CNN, RetinaNet is divided into two modules: a residual network (ResNet) as an encoder and a resource pyramid network (FPN) as a decoder, with ResNet being a model formed in a pyramid of resources, in various scales and parallel executions, thus performing convolutional operations, divided into layers that will be used by the FPN decoder. SABL is a network proposed as a more efficient way to detect objects with more precision than conventional methods, where each side of the image boundary is identified as a dedicated network branch, that is, several divisions are made in the target object where it will be identified and analyzed individually. The ATSS, called network with anchor, performs this selection according to the statistical characteristics of the object, that is, an analysis of the data received to identify whether they will be used in the training and testing dataset in detecting the object or not. It performs calculations throughout the image and analyzes the points of importance, of excellent quality and which differ particular elements from others, adding a margin of 50.7% AP in state-of-the-art detectors with no processing impact.

Based on ATSS + FCOS architecture, VFNet, or VarifocalNet, is a network with the projection of a new loss function and refinements in bounding boxes.

3.3 Statistical Analysis

With our dataset created and the networks models trained, the final step consisted to test and analyze the results generated. The evaluation of how well the predictions have been made with the mean Average Precision (mAP), which was the most common metric used by object detection challenges, and used the concepts of precision and recall in conjunction with the Interception over Union (IoU) to score the prediction [25]. Other commonly used metrics are Precision, Recall, Accuracy and F-Score (or F1-Score) [26, 27], where Accuracy (Acc) can be defined as the ability of a model to identify objects correctly, Precision (P) can be defined as the ability of a model to identify only relevant objects and Recall (R) can be defined as the ability of a model to identify all relevant cases and they can be mathematically defined as:

$$Acc = \frac{TP+TN}{TP+FP+TN+FN}, \tag{1}$$

$$P = \frac{TP}{TP+FP}, \; R = \frac{TP}{TP+FN}, \tag{2}$$

where *TP* (True Positive) is a correct object detection, *FP* (False Positive) is an incorrect detection of a nonexistent object or a misplaced detection of an existing object, *TN* (True Negative) when no detection is made and *FN* (False Negative) is an undetected object.

We can measure the success rate of the classifier by defining F-score as the harmonic mean of P and R as:

$$\text{F-Score} = 2\frac{PR}{P+R} = \frac{2TP}{2TP+FP+FN}, \tag{3}$$

By comparing the IoU result with a threshold t, we can classify if a detection is correct (if IoU $\geq$ t) or incorrect (if IoU $<$ t), where this threshold can be 0.3, 0.5 or 0.75. Defined how to classify a correct or incorrect detection, we can see that an object detector can be considered good if it detects all ground-truth objects while identifying only relevant objects. A good object detector is one that maintains high accuracy while increasing recall values, which means that regardless of threshold variation, accuracy and recall should remain high. This can be visualized through the area under the precision $\times$ recall curve. Unfortunately, the area under the curve (AUC) is often a zigzag-like curve and a processing in the Average Precision (AP) is made as

$$AP = \sum_n (R_{n+1} - R_n) P_{interp}(R_{n+1}) \tag{4}$$

where, $P_{interp}(R_{n+1}) = max_{R:R \geq R_{n+1}} P(R)$. Finally, we can calculate the mean Average Precision (mAP) as:

$$mAP = \frac{1}{N}\sum_{i=1}^{N} AP_i, \tag{5}$$

with AP_i being the AP in the ith class and N is the total number of classes being evaluated. For clarity, the AP can be evaluated with different IoUs thresholds, 0.5 or 0.75, and, for each, we call it AP50 or AP75, respectively. We can also evaluate the AP by averaging 10 different IoUs thresholds, beginning in 0.5 and ending in 0.95, with steps of 0.05, this will be called AP.

4. Results and Discussion

The results of the first phase showed that the RetinaNet and VFNet did not learn to identify the dogs' noses, which is reflected in their poor performance in all metrics (precision, recall, F-score, and mAP), which can be seen in Table 1. Consequently, they were discarded from further evaluation. Faster R-CNN achieved strong overall performance, with a particularly high recall, meaning it could detect most instances of the target object, though with slightly lower precision compared to others. ATSS had perfect precision, but its recall was significantly lower. This means it correctly identified the nose when detected but failed to detect it in many instances, leading to a lower F-score. However, it achieved the highest values for mAP and mAP75, indicating superior performance when the Intersection over Union (IoU) threshold is higher, meaning it excelled in detecting the object more precisely when detected. SABL also performed well, with a strong balance between precision and recall. Its precision was higher than Faster R-CNN, but its recall and F-score were slightly lower. In terms of mAP metrics, it also performed well, though it didn't surpass ATSS in mAP.

Table 1. Mean 5-fold nose detection results in the dataset for Faster R-CNN, SABL, RetinaNet, VFNet, and ATSS. The standard deviation value is displayed in parentheses.

CNN	Precision	Recall	F-Score	Accuracy
Faster R-CNN	95% (7%)	**94% (3%)**	**95% (4%)**	**92%**
RetinaNet	0% (0%)	0% (0%)	0% (0%)	0%
ATSS	**100% (0%)**	56% (17%)	70% (14%)	57%
VFNet	0% (0%)	0% (0%)	0% (0%)	0%
SABL	97% (4%)	90% (6%)	93% (3%)	90%

The same can be seen in Table 2, where the RetinaNet and VFNet networks did not obtain good results for mAP, mAP50 and mAP75, which resulted in their discarding in the next phase of the research. Although it had the lowest value for Recall and F-Score, ATSS obtained the highest values for mAP and mAP75, which means that it has the better results than the other networks when the Intersection over Union is higher.

Figure 3 shows the boxplot for the mAP metrics (mAP, mAP50, mAP75) and it can be seen that the boxplot of all

Table 2. Mean 5-fold for mAP, mAP50 and mAP75 results in the dataset. The standard deviation value is displayed in parentheses.

CNN	mAP	mAP50	mAP75
Faster R-CNN	0.544 (0.018)	**0.957 (0.027)**	0.530 (0.039)
RetinaNet	0.000 (0.000)	0.000 (0.000)	0.000 (0.000)
ATSS	**0.562 (0.028)**	0.943 (0.028)	**0.655 (0.131)**
VFNet	0.000 (0.000)	0.000 (0.000)	0.000 (0.000)
SABL	0.544 (0.022)	0.953 (0.022)	0.559 (0.107)

Table 3. Second phase results for Faster R-CNN, ATSS and SABL.

CNN	Precision	Recall	F-Score	Accuracy
Faster R-CNN	**100%**	89%	94%	89%
ATSS	**100%**	62%	76%	62%
SABL	97%	**95%**	**96%**	**91%**

metrics is 0 for the RetinaNet and VFNet networks in contrast to the good performance shown by Faster R-CNN, ATSS and SABL networks.

The results of the second phase showed that SABL obtained the highest values in all metrics, except in Precision, having 97% of Precision against 100% of Faster R-CNN and ATSS (Table 3). However, Faster R-CNN obtained values above 90% for Precision (95%), Recall (93%), F-Score (94%) and accuracy (97%). Table 4 shows that SABL was superior in mAP50 and mAP75, being inferior only to ATSS in mAP.

Figure 4 shows the boxplot for mAP metrics (mAP, mAP50, mAP75) and shows that the results obtained by SABL are better than those obtained by Faster R-CNN and ATSS.

As shown in Figure 5, ATSS found markings closest to the nostril, better than the human annotations in some cases, giving it the best result for mAP, although it could not find the nostril in every image from our dataset. Faster R-CNN and SABL found the nostril in almost every image from our dataset, but with a wider mark, and one false positive from SABL. However, SABL obtained the highest values for mAP50, mAP75, Recall, F-Score and Accuracy, narrowly losing in Precision and in mAP.

In the second phase, SABL proved to be the most consistent, achieving the highest values in most metrics (Recall, F-Score, Accuracy, mAP50, and mAP75). The only areas where SABL fell short were in precision (97% vs. 100% for Faster R-CNN and ATSS) and overall mAP, where ATSS had the edge. Faster R-CNN continued to perform reliably, with high precision, recall, F-score, and accuracy. Although it was slightly outperformed by SABL in mAP metrics, its results were strong across the board. ATSS stood out for its mAP, particularly at higher IoU thresholds, but it struggled in recall and F-score compared to the other models. The boxplot visualization confirmed ATSS's tendency to have superior mAP performance when detecting markings close to the nostrils, sometimes even better than human annotations, but it missed some instances of the nose, lowering its overall effectiveness.

Table 4. Second phase results for mAP, mAP50 and mAP75 in Faster R-CNN, ATSS and SABL.

CNN	mAP	mAP50	mAP75
Faster R-CNN	0.455	0.938	0.240
ATSS	**0.470**	0.932	0.265
SABL	0.458	**0.951**	**0.344**

5. Conclusion

Due to the increase in families with pets and the large movement of people concerned about their pet's well-being, this work presented a new technology that aims to detect the nose of bulldogs. With the nose detected, we can analyze the nostrils, looking for anatomical irregularities and airway diseases. Five networks were used for training in the first phase, Faster R-CNN, SABL, RetinaNet, VFNet, and ATSS, and three networks in the second phase, ATSS, Faster R-CNN and SABL. ATSS achieved the highest values for mAP and Precision during both phases, indicating its superior performance in terms of exact and confident detections of the bulldog's nose. This makes it effective when precision is critical, particularly for tasks requiring high Intersection over Union (IoU) values. SABL, however, demonstrated the best overall performance by the end of the second phase. It achieved the highest values for mAP50 and mAP75, Recall, F-Score and Accuracy. These results highlight SABL's balanced performance, making it the most reliable network for comprehensive detection tasks where recall, accuracy, and broader identification of the bulldog's nose (including edge cases) are important.

Acknowledgements

We thank Dom Bosco Catholic University (UCDB), Conselho Nacional de Desenvolvimento Científico e Tecnologico (CNPq), Fundação de Apoio ao Desenvolvimento do Ensino, Ciencia e Tecnologia do estado de Mato Grosso do Sul (FUNDECT), NVIDIA Corporation for the donation of the graphics card, Fundacção de Amparo à Pesquisa do Estado de São Paulo (FAPESP) and Embrapa Agricultura Digital/CNPTIA/EMBRAPA.

Author contributions

The lead author Joyce Katiuccia Medeiros Ramos Carvalho, Sandra Adriana Uhry and Gisele Braziliano de Andrade were responsible for the starting plan, the test dataset and its accuracy, and for writing and reviewing the paper. The authors Pedro Henrique Neves da Silva and Gustavo da Silva Andrade developed the code and wrote the paper. Authors Newton Loebens and Hemerson Pistori participated in the conception of the ideas and in the supervision and review of the papers.

References

[1] Fonfara, Sonja, de la Heras Alegret, Lourdes, German, Alexander J., Blackwood, Laura, Dukes-McEwan, Joanna, Noble, P.J. M., Burrow, Rachel D. (2011). Underlying diseases in dogs referred to a veterinary teaching hospital

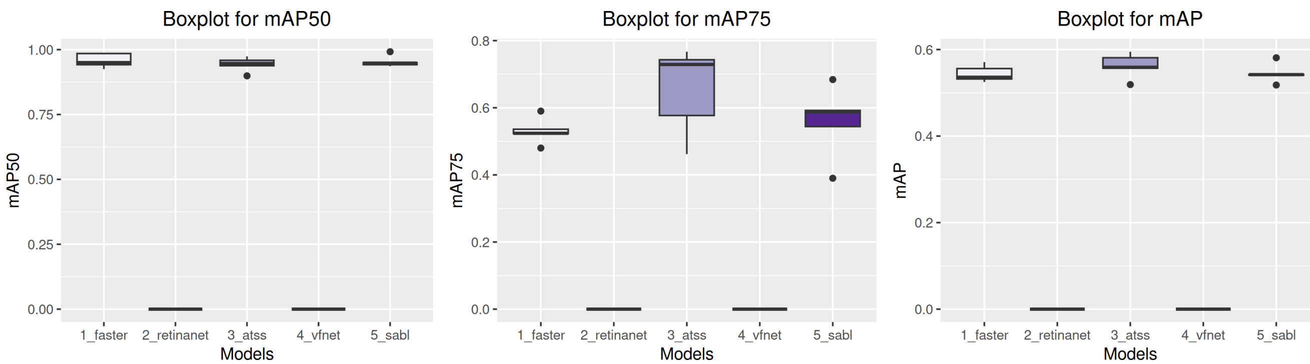

Figure 3. Evaluation metrics (mAP, mAP50 and mAP75) in boxplot.

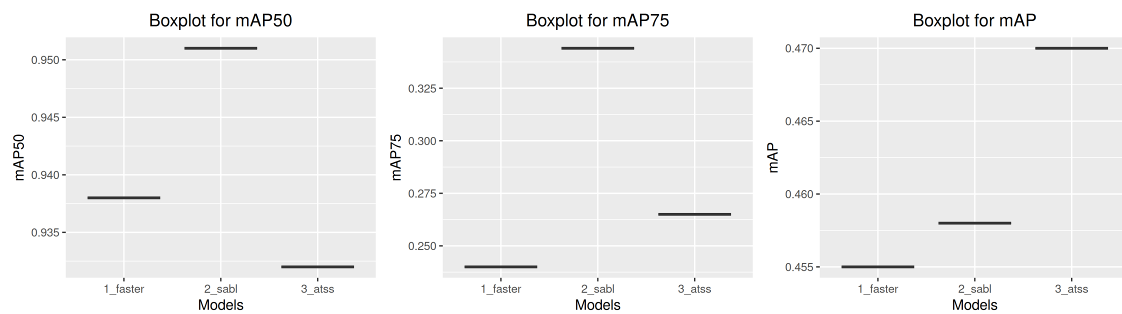

Figure 4. Evaluation metrics (mAP, mAP50 and mAP75) in boxplot.

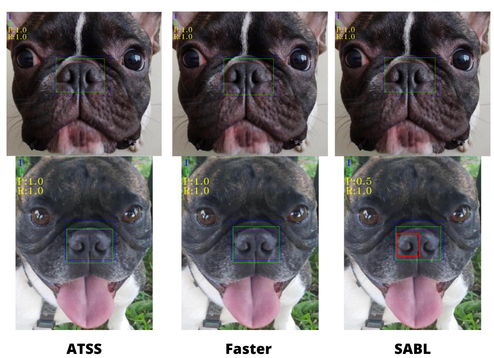

Figure 5. Results obtained from our dataset. Each column has boxes and numbers in blue denoting the human markings of the dog's nose region and the amount of marked objects. The boxes and numbers in green and in red are the objects found by the neural network and their quantity.

because of dyspnea: 229 cases (2003–2007). *Journal of the American Veterinary Medical Association*, 239(9), 1219–1224.

[2] Ren, S., He, K., Girshick, R., Sun, J. (2017). Faster R-CNN: Towards Real-Time Object Detection with Region Proposal Networks. *IEEE Transactions on Pattern Analysis and Machine Intelligence*, 36(6), 1137–1149. ⟨https://doi.org/10.1109/TPAMI.2016.2577031⟩

[3] Ren, Y., Zhu, C., Xiao, S. (2018). Small object detection in optical remote sensing images via modified faster R-CNN. *Applied Sciences*, 8(5), 813. ⟨https://doi.org/10.3390/app8050813⟩

[4] Wang, Jiaqi, Zhang, Wenwei, Cao, Yuhang, Chen, Kai, Pang, Jiangmiao, Gong, Tao, Shi, Jianping, Loy, Chen Change, Lin, Dahua. (2019, December). Side-Aware Boundary Localization for More Precise Object Detection.

[5] Berrar, Daniel. (2018, January). Cross-Validation. In *Cross-Validation*, ISBN: 9780128096338. ⟨https://doi.org/10.1016/B978-0-12-809633-8.20349-X⟩

[6] Anguita, Davide, Ghio, Alessandro, Ridella, Sandro, Sterpi, Dario. (2009, January). K-Fold Cross Validation for Error Rate Estimate in Support Vector Machines. *In Proceedings of the ...*, 291-297.

[7] Hoang, Toan, Nguyen, Phong, Truong, Noi, Lee, Young, Park, Kang. (2019, January). Deep RetinaNet-Based Detection and Classification of Road Markings by Visible Light Camera Sensors. *Sensors*, 19, 281. ⟨https://doi.org/10.3390/s19020281⟩

[8] Lin, Tsung-Yi, Goyal, Priya, Girshick, Ross, He, Kaiming, Dollar, Piotr. (2017, October). Focal Loss for Dense Object Detection. ⟨https://doi.org/10.1109/ICCV.2017.324⟩

[9] Zhang, Shifeng, Chi, Cheng, Yao, Yongqiang, Lei, Zhen, Li, Stan. (2020, June). Bridging the Gap Between Anchor-Based and Anchor-Free Detection via Adaptive Training Sample Selection. ⟨https://doi.org/10.1109/CVPR42600.2020.00978⟩

[10] Bannasch, Danika, Young, Amy, Myers, Jeffrey, Truvé, Katarina, Dickinson, Peter, Gregg, Jeffrey, Davis, Ryan, Bongcam-Rudloff, Eric, Webster, Matthew T., Lindblad-Toh,

Kerstin, et al. (2010). Localization of canine brachycephaly using an across breed mapping approach. *PloS one*, 5(3), e9632. ⟨https://doi.org/10.1371/journal.pone.0009632⟩

[11] Lilja-Maula, Liisa, Lappalainen, Anu K., Hyytiäinen, Heli K., Kuusela, Erja, Kaimio, Mirja, Schildt, Kirsti, Mölsä, Sari, Morelius, Mikael, Rajamäki, Minna M. (2017). Comparison of submaximal exercise test results and severity of brachycephalic obstructive airway syndrome in English bulldogs. *The Veterinary Journal*, 219, 22–26.

[12] Dupré, Gilles, Heidenreich, Dorothee. (2016). Brachycephalic syndrome. *Veterinary Clinics: Small Animal Practice*, 46(4), 691–707.

[13] Allemand, Vanice Correto Dutra, Quinzani, Marcelo, Berl, Carla Alice. (2013). Síndrome respiratória dos cães braquicefálicos: relato de caso. *Revista de Educação Continuada em Medicina Veterinária e Zootecnia do CRMV-SP*, 11(2), 42–47.

[14] Sławuta, P., Nicpoń, J., Domańska, S. (2011). Influence of the wing-of-the-nostrils correction procedure on the change of the acid-base balance parameters and oxygen concentration in the arterial blood in French bulldogs. *Polish journal of veterinary sciences*.

[15] Fasanella, Frank J., Shivley, Jacob M., Wardlaw, Jennifer L., Givaruangsawat, Sumalee. (2010). Brachycephalic airway obstructive syndrome in dogs: 90 cases (1991–2008). *Journal of the American Veterinary Medical Association*, 237(9), 1048–1051.

[16] Mitze, S., Barrs, V. R., Beatty, J. A., Hobi, S., Beczkowski, P. M. (2022). Brachycephalic Obstructive Airway Syndrome: much more than a surgical problem. *The veterinary quarterly*.

[17] Kenny, Dan D., Freemantle, Rosie, Jeffery, Andrea, Tivers, Michael S. (2022). Impact of an educational intervention on public perception of brachycephalic obstructive airway syndrome in brachycephalic dogs. *Veterinary Record*, 190(11), e1430. ⟨https://doi.org/10.1002/vetr.1430⟩

[18] Koch, Daniel A., Arnold, Susanne, Hubler, Madeleine, Montavon, Pierre M. (2003). Brachycephalic syndrome in dogs. *Compendium on Continuing Education for the Practising Veterinarian-North American Edition*, 25(1), 48–55.

[19] Liu, Nai-Chieh, Sargan, David R., Adams, Vicki J., Ladlow, Jane F. (2015). Characterisation of brachycephalic obstructive airway syndrome in French bulldogs using whole-body barometric plethysmography. *PLoS One*, 10(6), e0130741. ⟨https://doi.org/10.1371/journal.pone.0130741⟩

[20] Liu, Nai-Chieh, Troconis, Eileen L., Kalmar, Lajos, Price, David J., Wright, Hattie E., Adams, Vicki J., Sargan, David R., Ladlow, Jane F. (2017). Conformational risk factors of brachycephalic obstructive airway syndrome (BOAS) in pugs, French bulldogs, and bulldogs. *PloS one*, 12(8), e0181928. ⟨https://doi.org/10.1371/journal.pone.0181928⟩

[21] Liu, N-C., Adams, V.J., Kalmar, Lajos, Ladlow, J.F., Sargan, D.R. (2016). Whole-body barometric plethysmography characterizes upper airway obstruction in 3 brachycephalic breeds of dogs. *Journal of veterinary internal medicine*, 30(3), 853–865.

[22] Oechtering, Gerhard U., Pohl, Sabine, Schlueter, Claudia, Lippert, Johanna P., Alef, Michaele, Kiefer, Ingmar, Ludewig, Eberhard, Schuenemann, Riccarda. (2016). A novel approach to brachycephalic syndrome. 1. Evaluation of anatomical intranasal airway obstruction. *Veterinary Surgery*, 45(2), 165–172.

[23] Packer, Rowena M.A., Tivers, Michael S. (2015). Strategies for the management and prevention of conformation-related respiratory disorders in brachycephalic dogs. *Veterinary Medicine: Research and Reports*, 6, 219.

[24] Roedler, Frauke S., Pohl, Sabine, Oechtering, Gerhard U. (2013). How does severe brachycephaly affect dog's lives? Results of a structured preoperative owner questionnaire. *The Veterinary Journal*, 198(3), 606–610.

[25] Padilla, Rafael, Netto, Sergio L., da Silva, Eduardo A.B. (2020). A Survey on Performance Metrics for Object-Detection Algorithms. In *2020 International Conference on Systems, Signals and Image Processing (IWSSIP)*, 237-242. ⟨https://doi.org/10.1109/IWSSIP48289.2020.9145130⟩

[26] Lipton, Zachary Chase, Elkan, Charles, Narayanaswamy, Balakrishnan. (2014). Thresholding classifiers to maximize F1 score. *arXiv preprint arXiv:1402.1892*.

[27] Baratloo, Alireza, Hosseini, Mostafa, Negida, Ahmed, El Ashal, Gehad. (2015). Part 1: simple definition and calculation of accuracy, sensitivity and specificity. *ARCHIVES OF ACADEMIC EMERGENCY MEDICINE (EMERGENCY)*.

[28] Biercher, Anika, Meller, Sebastian, Wendt, Jakob, Caspari, Norman, Schmidt-Mosig, Johannes, De Decker, Steven, Volk, Holger Andreas. (2021). Using deep learning to detect spinal cord diseases on thoracolumbar magnetic resonance images of dogs. *Frontiers in veterinary science*, 8.

[29] Dac, Hai Ho, Gonzalez Viejo, Claudia, Lipovetzky, Nir, Tongson, Eden, Dunshea, Frank R., Fuentes, Sigfredo. (2022). Livestock Identification Using Deep Learning for Traceability. *Sensors*, 22(21), 8256. ⟨https://doi.org/10.3390/s22068256⟩

[30] Chen, Peng, Swarup, Pranjal, Matkowski, Wojciech Michal, Kong, Adams Wai Kin, Han, Su, Zhang, Zhihe, Rong, Hou. (2020). A study on giant panda recognition based on images of a large proportion of captive pandas. *Ecology and Evolution*, 10(7), 3561–3573. ⟨https://doi.org/10.1002/ece3.6190⟩

[31] Li, Guoming, Erickson, Galen E., Xiong, Yijie. (2022). Individual Beef Cattle Identification Using Muzzle Images and Deep Learning Techniques. *Animals*, 12(11), 1453.